SENSITIVITY TO MORPHOLOGY IN URBAN BOUNDARY LAYER MODELING AT THE MESOSCALE

David D. Flagg* and Peter A. Taylor
York University, Toronto, Ontario, Canada

1. INTRODUCTION

The representation of urbanized surfaces in a mesoscale numerical weather prediction (NWP) model poses a formidable challenge in dynamics and thermodynamics. The heterogeneity of surface type generally precludes explicit solution, requiring parameterization of physical processes to understand the meteorology of the urban boundary layer (UBL). These processes include radiative transfer, drag from buildings, anthropogenic heat flux as well as the transport of turbulent quantities of heat and momentum and their exchange with the inertial layer above (see Figure 1). To parameterize these physical processes, mesoscale modeling of the urban environment (resolution scale ~ $O(10^2\text{-}10^4)$) requires parameterization of its form, or morphology. Morphology representation entails averaging key geometric quantities such as roughness element (building) dimensions, building density and fractional surface coverage by anthropogenic material. At the mesoscale, this method of morphology representation does not resolve individual structures, thus introducing sub-grid scale variation. This study seeks to evaluate the sensitivity of pertinent atmospheric quantities in the urban boundary layer to small perturbations in key urban morphological parameterizations using the NCEP/NCAR Weather Research and Forecasting Model (WRF) and its newly coupled urban canopy model (UCM: Kusaka and Kimura 2004).

Uncertainty in the initial and boundary conditions of an NWP model may derive from sub-grid scale variation, incomplete model physics, measurement error or other sources. The typically heterogeneous urban morphology contributes substantially to sub-grid scale variation in the description of the model surface. A common response to this problem is to classify surface aggregates according to a dominant structural form such as "high-intensity residential" or "commercial." This allows for the creation of a set of categorical urban land surface types, each with distinct physical and thermal characteristics (Grimmond and Oke 1999). However, sub-grid scale variations in morphology remain. Many relevant

meteorological quantities, such as urban canopy wind speed, urban boundary layer depth, turbulence kinetic energy, heat flux, street canyon air temperature, etc., all derive from parameterizations influenced by the urban morphology. Of crucial interest to urban environmental modeling is pollutant transport, of which a viable short-term forecast depends on accurate model estimates of the meteorology (Dabberdt et al. 2004, Fisher et al. 2006, Hess et al. 2004, Taha and Bornstein 2000). Thus, urban air quality studies are inevitably subject to the uncertainty caused by sub-grid scale variations in urban morphology representations. Current remote sensing and geographic information systems (GIS) techniques can provide a very accurate, high-resolution depiction of the urban environment (Hafner and Kidder 1999, Rotach et al. 2005). However, the integration of such data into an operational NWP model may be costly
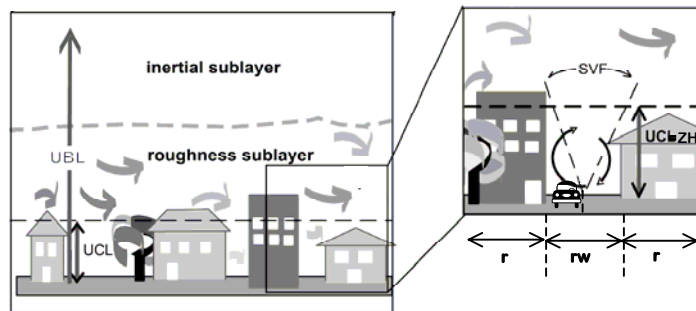
Figure 1: Schematic diagram of the urban boundary layer (UBL) illustrating the urban canopy layer (UCL) corresponding here to the mean structural height (ZH). Also shown are the sky view factor (SVF), normalized mean building width (R) street canyon width (RW), where R+RW=1 in the WRF-UCM representation of the urban surface. Adapted from Fisher et al. (2006).

and spatially limited. Therefore, it is important to understand the sensitivity of urban meteorology to uncertainties in the parameterized urban morphology to demonstrate the limitations in deterministic NWP forecasts of the UBL for meteorological and air quality concerns.

In this experiment, the principal user-defined morphology parameters driving WRF-UCM: mean structural height (z_r), normalized building (r) and road width (rw), the fractional surface coverage by anthropogenic material (hereinafter: "urban fraction (f_{URB})") and the building drag coefficient (C_D) are each perturbed by ± 10 percent in separate tests in a domain covering the Detroit-Windsor metropolitan area (U.S.A-Canada). These perturbations conservatively reflect common sub-grid scale variations in mesoscale urban

* *Corresponding author address*: David D. Flagg, York University, Department of Earth and Space Science and Engineering – Centre for Research in Earth and Space Science (CRESS), Toronto, Ontario, Canada M3J 1P3; email: dflagg@yorku.ca

morphology parameterirzations (Grimmond and Oke 1999). Early results presented here focus exclusively on the meteorological response during the growth of the atmospheric boundary layer (ABL) on a summer day dominated by buoyant turbulent production (free convection). These results provide a preliminary quantitative estimate of the potential variation in the ABL meteorology manifested through sub-grid scale variation in the urban morphology. On-going and future work will complete this study with analysis of the nocturnal response and the response under an idealized urban environment. Section 2 outlines the experimental method, including a review of the WRF model and its coupled UCM as well as a description of its implementation at Detroit-Windsor. Section 3 provides preliminary results of the case studies introduced in Section 2. Conclusions and a brief discussion of on-going and future work follow in Section 4.

2. METHOD

2.1. Model

2.1.1. Weather Research and Forecasting Model

The Weather Research and Forecasting Model (WRF) is a mesoscale numerical weather prediction and data assimilation modeling system produced as a joint venture of the (U.S.) National Oceanic and Atmospheric Administration (NOAA) National Centers for Environmental Prediction (NCEP) and Forecast System Laboratory (FSL) and the (U.S.) National Center for Atmospheric Research (NCAR) plus additional collaboration with the (U.S.) Department of Defense Air Force Weather Agency (AFWA), the Naval Research Laboratory (NRL), the University of Oklahoma Center for Analysis and Prediction of Storms (CAPS) and the Federal Aviation Administration (FAA). It is designed to satisfy the needs of both the research and operational forecasting communities and provides the user with copious options for physical and numerical parameterization. The model is built for easy configuration to a broad array of serial and parallel computing environments.

This study invokes the Advanced Research (ARW) version 2.2 dynamical core option (Skamarock et al. 2007), which provides a fully compressible governing equation set in an Eulerian framework that solves prognostic three-dimensional wind, perturbation geopotential, perturbation potential temperature and perturbation surface pressure of dry air plus optional scalars (e.g., water vapor mixing ratio). This study invokes the non-hydrostratic option, as is appropriate for a mesoscale resolution. The vertical grid spacing is stretchable and user-specified according to a terrain-following, hydrostatic vertical coordinate with a constant pressure, gravity-wave absorbing lid. Model variables are aligned in the horizontal according to the Arakawa-C grid. The model time integration uses a third-order Runge-Kutta scheme; the spatial discretization uses 2nd to 6th order schemes in both the horizontal and vertical.

The model functions in both 'real' and 'idealized' settings; this study invokes the 'real' configuration and uses NCEP Eta 212 grid (40km) model analysis (a.k.a., 'AWIP'), data to satisfy initial and boundary conditions. The AWIP set includes eight sets of three-dimensional and surface analyses daily at 26 vertical levels from 1000 hPa to 50 hPa. The set (ds609.2) is freely available from the University Corporation for Atmospheric Research (UCAR) and is updated frequently with recent data. The WRF Pre-Processor System (WPS) serves to ingest and interpolate surface and three-dimensional boundary and initial conditions for 'real' case applications from a wide variety of commonly used model analyses (such as AWIP, ECMWF, GFS, NARR, etc.).

WRF provides the user with a suite of options for parameterizing various physical processes such as microphysics, cumulus parameterization, land surface physics, ABL physics and atmospheric radiation physics. Table 1 lists the physics parameterizations selected for this study.

Physical Process	Selected Scheme
Microphysics	WRF Single Moment 6-class (WSM6)
Cumulus Parameterization	Kain-Fritsch (Kain and Fritsch 1993); coarsest domain only
Longwave Radiation	Rapid Radiative Transfer Model (RRTM) (Mlawer et al. 1997)
Shortwave Radiation	Goddard shortwave radiation (Chou and Suarez 1994)
Land Surface Physics	Noah land surface model (Chen and Dudhia 2001)
ABL Physics	Mellor-Yamada-Janjic (MYJ) (Janjic 2002)

Table 1: Selection of physical parameterizations implemented in local WRF installation

These choices largely reflect constraints imposed by the intended grid scale (see Section 2.2) and required complexity, according to recommendations from the WRF User Guide (Skamarock et al. 2007). Note that implementation of the UCM in WRF-ARW v2.2 requires the use of the Noah land surface model (LSM), described in Section 2.1.3.

The ABL physics parameterization options include the Yonsei University (YSU) scheme (Hong and Dudhia 2003) and the Mellor-Yamada-Janjic (MYJ) scheme (Janjic 2002). Numerous studies exist comparing the performance of these two schemes across a variety of WRF model integrations (Pagowski 2004, Pagowski et al. 2006, Chiao 2006). Results from these studies are mixed, but share in the suggestion of an overestimation of afternoon temperature and ABL depth from the YSU-Noah coupling. Off-line preliminary sensitivity testing with both ABL schemes reveals a slightly better fit of

ABL depth estimates with MYJ when matched against a series of summer season radiosonde profiles from a station within the study domain (see Section 2.2). The MYJ scheme also exhibits greater sensitivity to the presence of the UCM and to vertical resolution (of importance in the lower levels when tall buildings 'overlap' the lowest model layer under excessive vertical resolution). The MYJ scheme also offers extra functionality by providing turbulence kinetic energy (TKE) estimates at each vertical level. Thus, the MYJ ABL scheme is selected for this study.

2.1.2. Mellor-Yamada-Janjic Scheme

The Mellor-Yamada-Janjic (MYJ) scheme (Janjic 2002) is an implementation of the Mellor-Yamada level 2.5 turbulence closure model (Mellor and Yamada 1982). To this model, an upper limit is imposed on the master length scale (ℓ). The latter is parameterized to prevent singularity in turbulence kinetic energy (TKE) production for unstable cases and to restrict the size of the ratio of vertical velocity deviation variance to TKE in stable cases. Janjic (2002) also updates several empirical constants.

The model iteratively solves the prognostic TKE differential equation at each model layer:

$$\frac{d\left(\frac{q^2}{2}\right)}{dt} - \frac{\partial}{\partial z}\left(\ell\, q\, S_q\, \frac{\partial\left(\frac{q^2}{2}\right)}{\partial z}\right) = P_s + P_b - \varepsilon \qquad (1),$$

$$P_s = K_M\left(\frac{\partial U}{\partial z}\frac{\partial U}{\partial z} + \frac{\partial V}{\partial z}\frac{\partial V}{\partial z}\right) \qquad (1a),$$

$$P_b = -\beta\, g\, K_H\left(\frac{\partial \theta_v}{\partial z}\right) \qquad (1b),$$

$$\varepsilon = \frac{q^3}{B_1\, \ell} \qquad (1c),$$

where $\frac{q^2}{2}$ is the TKE, K_M (K_H) is the vertical turbulent exchange coefficient for momentum (heat), $S_q = 0.20$, $\beta = 1/273$, B_1 is an experimental constant and all other symbols have common meanings. The shear production (P_s), buoyant production (P_b) and dissipation (ε) and a small vertical diffusion term comprise the components of the prognostic TKE. A threshold of TKE = 0.2 m^2 s^{-2} determines the top of the ABL.

Coupled with this ABL scheme is the Eta surface layer (SL) model, which iteratively computes the $\Psi(\zeta)$ functions of Monin-Obukhov similarity theory (MOST:

Monin and Obukhov 1954) from a range of ζ (default is $-5 < \zeta < 1$) where (ζ)=z/L where L is the Obukhov length scale and z is height above ground level (AGL). The Eta SL also invokes Zilitinkevitch (1995) in defining the viscous sublayer parameterization using the roughness length (z_0). The Eta-SL distinguishes roughness lengths for heat and momentum.

2.1.3. Noah Land Surface Model

The Noah land surface model (LSM) derives from Chen and Dudhia (2001). It is a one-dimensional model that updates skin (surface) temperature and solves soil temperature and moisture at four sub-surface layers. It also calculates canopy moisture and passes canopy heat and moisture fluxes to the SL model (see Section 2.1.2). The Noah LSM also accounts for single layer snow cover and vegetation processes (when accompanied with an appropriate land surface classification map).

2.1.4. Urban Canopy Model

The WRF ARW v2.2 urban canopy model (UCM) (Kusaka and Kimura 2004) parameterizes the urban environment as a single-layer canopy that estimates surface energy budgets and a single in-canopy wind speed. Designed as an extension to the Noah LSM (see Section 2.1.3), the canopy consists of two-dimensional street canyons of infinite length. The UCM solves energy budgets at three surfaces: the road, canyon walls, and rooftop (see Figure 2). A parameterization for mean canyon orientation and sky-view factor (SVF) combined with the diurnal variation of the solar azimuth angle permit the radiation scheme to account for shadows and reflection in the shortwave budget. In this study, a four-layer diffusion model (user choice) solves the skin temperature at each surface, with a zero-flux lower boundary condition on each surface (user choice).

Sensible heat flux from the rooftop (H_R) is solved according to MOST (Monin and Obukhov 1954) while the canyon wall sensible heat flux (H_W) and road sensible heat flux (H_G) use Jurges formula:

$$H_W = C_W(T_W - T_S) \qquad (2),$$

$$H_G = C_G(T_G - T_S) \qquad (3),$$

$$C_W = C_G = \begin{cases} 7.51 U_S^{0.78} & (U_S \geq 5\, ms^{-1}) \\ 6.15 + 4.18 U_S & (U_S < 5\, ms^{-1}) \end{cases} \qquad (4),$$
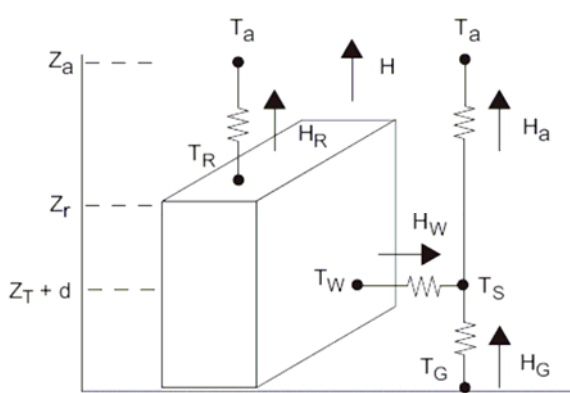
Figure 2: Schematic representation of the WRF UCM design and heat flux parameterization. T_a is the temperature at reference height z_a, T_R is the rooftop temperature, z_r is the mean building height, H_a is the combined, weighted heat flux from the urban canyon and all other terms follow from the text. (From Kusaka and Kimura 2004)

Where T_W, T_G are the temperatures of the canyon walls, and road, respectively, T_S is the air temperature at reference height $z_T + d$ (= roughness length for heat + displacement height), and U_S is a diagnostic wind speed at the reference height $z_T + d$.

The total canyon heat flux to the atmosphere above (H_a) is parameterized as a weighted sum of the wall and road heat fluxes:

$$rw \cdot H_a = 2 h_c H_W + rw \cdot H_G \qquad (5),$$

where h_c is the normalized building height. Finally, the total heat flux from the urban surface (H) is parameterized as a weighted sum of heat flux from all artificial surfaces (including the rooftop and canyon) (H_A)

$$H_A = r \cdot H_R + rw \cdot H_a \qquad (6),$$

and all natural surfaces (H_V) within the urban landscape:

$$H = f_{URB} H_A + (1 - f_{URB}) H_V \qquad (7),$$

Where H_V is the heat flux from the natural landscape, defined here as USGS category #5, "Cropland/Grassland Mosaic". Other total canopy fluxes, such as latent heat, ground heat and the net radiation budget are calculated similarly.

The canopy wind (U_c) is solved as an exponential profile:

$$U_C = U_a \frac{\ln\left[(z_a - d)/z_0\right]}{\ln\left[(z_r - d)/z_0\right]} \exp\left[-n\left(1 - \tfrac{z}{z_r}\right)\right] \qquad (8),$$

where z_0 is the roughness length for momentum, z_a is the height of the lowest atmospheric level above the urban canopy (see Figure 2), U_a is the horizontal wind at z_a, z is a reference height within the urban canopy (taken to be $0.7*z_r$ by default) and n is a function of the

volume occupied by buildings, the building drag coefficient and mixing length.

WRF-UCM requires a substantial list of gridded (i.e., changes with urban type) and non-gridded (i.e, universally applied) physical and thermodynamic parameters from the user. The non-gridded parameters (albedo, emissivity, heat capacity, thermal conductivity, layer thickness and moisture availability) require specification for all three surfaces (rooftop, canyon wall, road). This study applied the default values provided for all parameters with the exception of the latter (see Section 2.3). The gridded parameters mostly concern urban geometry and require additional consideration (see section 2.3).

Kusaka and Kimura (2004) demonstrate great improvement in the urban meteorology with the UCM versus a slab or 'sand box' representation (Myrup 1969). The model provides a thorough treatment of short and longwave radiation by incorporating urban geometry, shadows and sky-view factors. The representation of heat balance through three multi-layer surfaces provides detailed heat transfer estimation. Its portability to three-dimensional mesoscale NWP models, as here with WRF, also attests to its versatility and potential for future application.

2.2. Model Application to Domain

The experimental domain is the Detroit-Windsor metropolitan area, straddling the U.S.-Canada border, chosen as part of a regional study in air quality during the summer of 2007. Figure 3 illustrates the extent of the parent domain (1) and two two-way nested domains
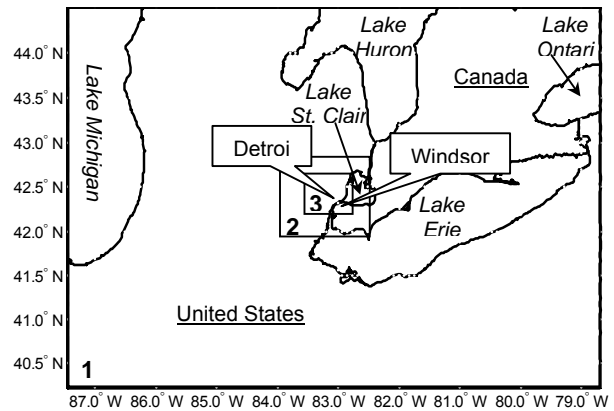
Figure 3: The study domain, centered over Detroit-Windsor, straddling the U.S.-Canada border, in the domain (3), nested within two coarser grids (2,1)

Domain	1	2	3
Gridpoints (zonal)	67	34	55
Gridpoints (meridional)	45	28	43
Horizontal grid scale (km)	15	5	1.67
Time step (s)	18	6	2

Table 2: Numerical specifications of study domains

(2, 3). The associated numerical design is shown in Table 2.

In a balance of stability and optimal resolution, the model resolves 35 vertical levels from the surface to 50 hPa including nine layers in the lowest kilometer. Martilli (2007) suggests that models estimating building drag through a roughness length set the midpoint of the lowest vertical layer above the roughness sublayer (RSL). Yang and Zhao (2006) reviews a series of accepted RSL parameterizations and follows Harman et al. (2004) to set $z_{RSL}=2\ z_r$. The first layer midpoint here averages around 23-25 m AGL.

The current focus of study concentrates on the daytime ABL, from the early morning through the afternoon collapse. Of particular interest in this sensitivity study is the meteorological response over the urban surface, as well as that over non-urban surfaces. Thus, the study requires one or more dry days with free-convection-dominated mixed layer growth and minimal background (i.e., synoptic) flow that would otherwise induce excessive shear stress on UBL development. Examination of surface analyses during the period June through August of 2007 yields two dates that optimally satisfy these conditions: 1 August and 23 June. Results here focus on 1 August for the period 08:00 – 20:00 local time (LT), (UTC - 4).

2.3. Enhancing Geography & UCM Parameters

WRF can accept any suitably configured geography dataset but is readily amenable to the United States Geological Survey (USGS) 24-category land surface category dataset with global coverage and available resolutions at 30", 2', 5' and 10'. This set classifies all urban grid cells as one category. Given the 1.67 km horizontal grid scale of the finest domain (see Table 2) and the high-resolution satellite imagery freely available and easily accessible from *Google Earth™ mapping service*, it is possible to manually re-classify urban grid cells to better reflect the spectrum of morphology across a metropolitan area in an effort to improve model performance (Ding et al. 2007).

Grimmond and Oke (1999) provide a useful range of standard urban morphology parameters for four classifications of urban surface. Following this approach, this study designates four urban categories: low intensity, medium intensity, high intensity and high-rise with parameters set as shown in Table 3. Using these parameters as a guide, the area of domain 2 is manually inspected for the presence of each urban type using building density, type and f_{URB}. Each discrete area

of the domain deemed to sufficiently meet the characteristics of a particular urban type (Grimmond and Oke 1999) is manually marked by an appropriately colored polygon annotated onto the map to indicate the local spatial limits of that urban type. When complete, a 30" grid is superposed onto the annotated map to overlap the grid of the 30" USGS land surface dataset. Each resultant 30" grid cell with one or more annotated polygons present within is evaluated to determine the (spatially) dominant urban type. Finally, the new map is blended with the original USGS 30" dataset to reflect the exchange of one urban type for four. The surface thermodynamic properties of these new types are set to the default single-category urban properties, which become redundant when the UCM is activated.

The implementation of the UCM requires user specification of a series of gridded parameterizations (Table 3). The building height, roughness length and displacement heights derive from mean values presented by Grimmond and Oke (1999). Normalized road and street width for low and medium intensity types derive from UCM default settings. The high intensity and high rise values derive from an average of samples taken within the domain. Normalized building height was calculated as a ratio of mean building height and geometric street and building widths (m), averaged from samples taken across the domain. The building drag coefficient follows from Brown (2000). The volumetric parameter follows from default UCM ratios. The urban fraction follows from UCM default settings and Makar et al. (2006). The only change made to the default non-gridded UCM parameterizations is to add a small moisture availability (0.10) to the road and rooftop surfaces for all urban types to account for potential standing rainwater, rooftop gardens, evapotranspiration from street canyon flora, washed sidewalks and other miscellaneous sources.

The parameterizations in Table 3 are labeled the "best fit" case. This preliminary study is composed of six tests comparing this case to a perturbation of one particular parameter in all urban types:

Urban Category	Building Height (m)	Roughness Length (m)	Displ. Height (m)	Norm. Building Width (-)	Norm. Street Width (-)	Norm. Building Height (-)	Drag Coeff. (-)	Building Volumetric Parameter (m^{-1})	Urban Fraction (-)
Low Inten.	7	0.7	3	0.50	0.50	0.35	0.05	0.3	0.50
Med Inten.	10	1.0	6	0.50	0.50	0.28	0.08	0.4	0.75
High Inten.	15	1.5	11	0.67	0.33	0.33	0.17	0.6	0.90
High Rise	20	2.0	15	0.75	0.25	0.33	0.19	0.8	0.95

Table 3: Urban canopy model parameterization settings for the "Best Fit" study case.

"Best Fit" versus ($\pm$ 10 percent) Perturbation in:

1) Building height (z_r)
2) Urban Fraction (f_{URB})
3) Normalized Building Width (r)
4) Building Drag Coefficient (c_D)
 . . . and. . .
5) "Best Fit" versus 'default'
6) "Best Fit" versus "no UCM"

where 'default' represents the default UCM parameters assigned to the USGS landuse type 'urban' if the UCM is implemented with no intervention of the parameters or 24-category USGS landuse dataset. The "no UCM" case is uses the standard single 'urban' category run without the presence of the UCM.

3. PRELIMINARY RESULTS

To evaluate the meteorological response to morphology parameterization perturbations, it is useful to investigate the ABL turbulence kinetic energy (TKE), canopy air temperature, canopy wind speed, the ABL depth and the local energy budget. Results here concentrate on only the finest grid (domain #3, see Figure 2), examining domain averages over both urban and non-urban surfaces.

3.1. Turbulence Kinetic Energy

Figure 4 presents snapshots of the TKE cross-section at 15:00 LT, extending from 16km northwest to 16 km southeast of downtown Detroit. Despite the noise in the surrounding rural and suburban areas, there is a clear development of enhanced TKE over the downtown core during the day with accompanying positive velocity (not shown). When evaluated as an average over all urban areas, the "best fit" case shows a reduction in TKE overall in comparison to the "no UCM" case (Figure 5a, 5b). Closer inspection of the dominant TKE components, including shear and buoyant production and dissipation, reveals a substantial reduction in buoyant turbulence production as the source for this discrepancy (Figure 6a, 6b).

Offline tests not shown here suggest that perturbations to the building height parameter do provoke appropriate variation in the shear production term (e.g., increased height = increased shear production). Among other parameter perturbations inducing a conspicuous response in the TKE budget is f_{URB}. A 10 percent increase in that parameter results in a roughly 10-20 percent increase in shear production of TKE in the lower UBL (Figure 7a). The response is particularly strong in the mid-late afternoon (7b).

3.2. Surface Energy Budget

The model solves the net radiation, sensible, latent and ground heat flux at the roof, wall and road surfaces to calculate the net canopy heat fluxes. The net radiation is the sum of sensible, latent and ground heat fluxes; no explicit storage term exists in the balance.

Nearly all of the required gridded and non-gridded UCM parameterizations directly influence the energy budget. The total surface energy budget is calculated by the (Noah) LSM as a weighted sum of the urban canopy and natural surface fluxes. Specifically, the f_{URB} parameter determines this ratio. Hereafter, the term "urban surface energy budget" will refer to the aggregate energy fluxes from both the artificial and natural surface components of the 'urban' grid cell.

Figure 8a (8b) presents the total surface energy budget over urban (non-urban) surfaces in the "best fit" case. Results clearly indicate a significantly enhanced ground heat flux that peaks approximately one hour earlier, qualitatively supported by results from Kusaka and Kimura (2004).

IThe ground heat flux is also the most sensitive of the urban surface energy budget components to perturbation in the urban morphology parameterization. Perturbations to both building height (Figure 9a) and normalized building width (Figure 9b) yield up to a 4 Wm^{-2} difference in ground heat flux, the latter also demonstrating similar sensitivity in afternoon latent heat flux. Once again, f_{URB} yields the greatest sensitivity of the parameter perturbations, provoking up to a 17 Wm^{-2} difference in ground heat flux and up to a 15 Wm^{-2} difference in latent heat flux, both around midday (Figure 9c).

3.3. ABL Depth

Urban morphology parameter perturbation tests yield limited variation in the daytime ABL depth. Figure 10 depicts an example perturbation case (f_{URB}). The difference between the "best fit" and "no UCM" cases is more substantial and indicates a slight reduction due to UCM implementation, as expected from the discrepancy in the TKE profiles (Figures 5a and 5b).

3.4. Canopy Temperature

The canopy temperature also demonstrates minimal response to perturbations in the urban morphology parameters, as shown in Figure 11 for the case of perturbed building height. This figure also illustrates the average 2 m temperature obtained from several surrounding METAR stations in the Detroit-Windsor area, used here for comparison with canopy air temperature. Results suggest a slight improvement in afternoon canopy temperature prediction versus the 'default' case.

3.5. Canopy Wind Speed

The canopy wind speed shows very little response to urban morphology parameter perturbations. Figure 12 presents the results of perturbation to the building drag coefficient parameter, of which the urban canopy wind speed parameterization (8) is a function. The weak canopy wind shown in Figure 12 confirm minimal background flow expected from surface synoptic analysis.

3.6. Temperature and Moisture Profiles

Comparison to vertical profile measurements in these preliminary results is limited to a single measurement from a sounding at 20:00 LT at KDTX (White Lake, MI) west of Detroit. Comparing the "best fit" and "no UCM" cases evaluated at the nearest model grid point, the former is shows improvement in the potential temperature profile overall (Figure 13 a, b). The "no UCM" case demonstrates better prediction of the water vapor mixing ratio profile, especially in the lowest 2 km (Figure 13 c,d).This latter discrepancy may be due to parameterization of moisture availability in the UCM and will require further study.

4. CONCLUSION

This study investigates mesoscale model response of critical atmospheric boundary layer (ABL) meteorology variables to systematic perturbations in selected parameters of morphology in an urban canopy model. The parameter perturbations arbitrarily reflect potential sub-grid scale variation at the mesoscale given an underlying single-assignment land-use type as well as potential error in land-use type diagnosis from GIS imagery. The study is applied to a real data case over the Detroit-Windsor (U.S.-Canada) metropolitan area. Preliminary results presented here focus on the response during a single period of daytime mixed layer growth with minimal background flow.

Analysis of turbulence kinetic energy (TKE) reveals that the presence of an urban canopy model (UCM) serves to reduce buoyant TKE production over urban grid cells. Further study is needed to evaluate the possible role of insufficient heat transfer and/or overestimation of near surface potential temperature in the UCM or ABL schemes. Perturbation studies confirm that increased building height and urban fraction lead to increased shear production of TKE, up to 10-20 percent in the lower ABL for a 10 percent increase. Of all the parameters tests, perturbations to the urban fraction provoke the greatest sensitivity in the total TKE profile in the ABL column when averaged over all urban grid cells in the domain.

Within the surface budget, ground heat flux averaged over urban grid cells is found to increase substantially compared to non-urban surfaces. Balance is achieved by way of reduction of the sensible and latent heat fluxes over urban grid cells. The enhanced daytime ground heat flux uptake decelerates the late afternoon reduction in latent and sensible heat flux. The ground heat flux is also the most sensitive of the three heat fluxes to morphology parameter perturbation when evaluated over urban surfaces. Perturbations of the urban fraction parameter again yield the greatest response in the urban surface energy budget; a 10 percent parameter perturbation yields a 15 percent or greater change in ground and latent heat flux in the early afternoon.

When compared against a radiosonde dataset in the lowest 3 km, the optimally adjusted ("best fit") case of UCM parameterization achieved closer coherence to potential temperature measurements than either the case with no UCM implemented or the case with default UCM settings. The case without a UCM performed best in the water vapor mixing ratio profile. Considerable additional study is needed to investigate model response across a variety of ABL stability regimes. Further consideration and experimentation with the UCM schemes is also necessary to better establish systematic bias and potential error resulting from missing physical processes in the parameterization.

On-going work and future work will study the nocturnal meteorological response to urban morphology parameter perturbation. Additionally, future work will model a more controlled, idealized urban environment where the mesoscale meteorological response can be more accurately assessed as a function of urban parameterization.

6. REFERENCES

Brown, M.J., 2000: Urban Parameterizations for Mesoscale Meteorological Models, *Mesoscale Atmospheric Dispersion*, Z. Boybeyi, Ed., WIT Press, Southampton, UK, 193-255.

Chen, F. and J. Dudhia, 2001: Coupling an advanced land-surface/hydrology model with the Penn State/NCAR MM5 modeling system. Part I: Model description and implementation. *Mon. Wea. Rev.*, **129**, 569-585.

Chiao, S., 2006: Performance of the Weather Research and Forecasting (WRF) Model Atmospheric Boundary Layer Schemes. Proceedings of the *25th Army Science Conference*, Orlando, Florida, USA, 27-30 November.

Chou, M.-D. and M.J. Suarez, 1994: An efficient thermal infrared radiation parameterization for use in general circulations models. NASA Tech. Memo. 104606, **3**, 85 pp.

Dabberdt, W.F., M.A. Carroll, D. Baumgardner, G. Carmichael, R. Cohen, T. Dye, J. Ellis, G. Grell, S. Grimmond, S. Hanna, J. Irwin, B. Lamb, S. Madronich, J. McQueen, J. Meagher, T. Odman, J. Pleim, H.P. Schmid and D. Westphal, 2004: Meteorological Research Needs for Improved Air Quality Forecasting: Report of the 11th Prospectus Development Team of

the U.S. Weather Research Program. *Bull. of the Amer. Met. Soc.*, **85**, 563-586.

Ding, W., F. Zhu and Y. Hao, 2007: Interactive 3D City Modeling using Google Earth and Ground Images. *Proceedings of the Fourth International Conference on Image and Graphics*, Los Alamitos, California, USA, 22-24 August, 849-854.

Fisher, B., J. Kukkonen, M. Piringer, M.W. Rotach and M. Schatzmann, 2006: Meteorology Applied to Urban Air Pollution Problems: Concepts from COST 715. *Atmos. Chem. and Phys.*, **6**, 555-564.

Grimmond, C. and T. Oke, 1999: Aerodynamic Properties of Urban Areas Derived from Analysis of Surface Form. *J. Applied Met.*, **38**, 1262-1292.

Hafner, J. and S. Kidder. 1999: Urban Heat Island Modeling in Conjunction with Satellite-Derived Surface/Soil Parameters. *J. Applied Met.,* **38**, 448-465.

Harman, I. N., Barlow, J.F. and S.E. Belcher, 2004: Scalar Fluxes from Urban Street Canyons. Part II: Modelling Study. *Boundary-Layer Met.*, **113**, 387-410.

Hess, G., K. Tory, M. Cope, S. Lee, K. Puri, P. Manins and M. Young, 2004: The Australian Air Quality Forecasting System. Part II: Case Study of a Sydney 7-Day Photochemical Smog Event. *J. Applied Met.,* **43**, 663-679.

Hong, S.Y. and J. Dudhia, 2003: Testing of a non-local boundary layer vertical diffusion scheme in numerical weather prediction applications. *20th Conference on Weather Analysis and Forecasting*, Seattle, Washington, USA, 18-23 October.

Janjic, Z.I., 2002: Nonsingular Implementation of the Mellor-Yamada Level 2.5 Scheme in the NCEP Meso model. NCEP Office Note No. 437, 61 pp.

Kain, J.S. and M. Fritsch, 1993: Convective parameterization for mesoscale models: The Kain-Fritsch scheme, *The representation of cumulus convection in numerical models*, K.A. Emanuel and D.J. Raymond, Eds., Amer. Meteor. Soc., 246 pp.

Kusaka, H. and F. Kimura, 2004: Coupling a Single-Layer Urban Canopy Model with a Simple Atmospheric Model: Impact on Urban Heat Island Simulation for an Idealized Case. *J. Met. Soc. Japan*, **82**, 67-80.

Makar, P.A., S. Gravel, V. Chrikov, K.B. Strawbridge, F. Froude, J. Arnold and J.Brooke, 2006: Heat Flux, Urban Properties, and Regional Weather. *Atmos. Env.*, **40**, 2750-2766.

Martilli, A., 2007: Current Research and Future Challenges in Urban Mesoscale Modelling. *Int. J. of Climatol.* **27**, 1909-1918.

Mellor, G.L. and T. Yamada, 1982: Development of a turbulence closure model for geophysical fluid problems. *Rev. Geophys. Space Phys.,* **20**, 851-875.

Mlawer, E.J., S.J. Taubman, P.D. Brown, M.J. Iacono and S.A. Clough, 1997: Radiative transfer for inhomogeneous atmosphere: RRTM, a validated correlated-k model for the longwave. *J. Geophys. Res.,* **102** (D14), 16663-16682.

Monin, A.S. and A.M. Obukhov, 1954: Basic laws of turbulent mixing in the surface layer of the atmosphere. *Contrib. Geophys. Inst. Acad. Sci.*, USSR, (**151**), 163-187 (in Russian).

Myrup, L., 1969: A numerical model of the UHI. *J. Applied Met.* **8**, 908-918.

Pagowski, M., 2004: Some Comments on PBL Parameterizations in WRF. *5th WRF Users' Workshop,* Boulder, Colorado, USA. 22-25 June.

Pagowski, M., J. Hacker and D. Rostkier-Edelstein, 2006: Behavior of WRF BL Schemes and Land Surface Models in 1-D Simulations during BAMEX. *7th WRF Users' Workshop*, Boulder, Colorado, USA. 19-22 June.

Rotach, M.W., R.Vogt, C. Bernhofer, E. Batchvarova, A. Christen, A. Clappier, B. Feddersen, S.-E. Gryning, H. Mayer, V. Mitev, T.R. Oke, E. Parlow, H. Richner, M. Roth, Y.-A. Roulet, D. Ruffieux, J. Salmond, M. Schatzmann, and J.A. Voogt, 2005: BUBBLE - an Urban Boundary Layer Project. *Theoretical Appl Climatol.*, **81**, 231 – 261.

Skamarock, W.C., J.B. Klemp, J.Dudhia, D.O. Gill, D.M. Barker, W. Wang and J.G. Powers, 2007: A Description of the Advanced Research WRF Version 2. NCAR Tech Note, NCAR/TN-468+STR. 88 pp.

Stull, R.B., 1988: An Introduction to Boundary Layer Meteorology. Kluwer Academic Publishers, Dordrecht, The Netherlands, 670 pp.

Taha, H. and R. Bornstein, 2000: Urbanization of meteorological models and implications on simulated heat island and air quality. Biometeorology and urban climatology at the turn of the millennium, WMO Report WMO/TD-No. 1026, 431-435.

Yang, Y. and Y. Shao, 2006: A Scheme for Scalar Exchange in the Urban Boundary Layer. *Boundary-Layer Met.*, **120**, 111-132.

Zilitinkevich, S.S., 1995: Non-local turbulent transport: Pollution dispersion aspects of coherent structure of convective flows, *Air Pollution III – Volume I. Air Pollution Theory and Simulation*, H. Power, N. Moussiopoulos and C.A. Brebbia, Eds., Computation Mechanics Publications, Southampton, U.K., 53-60.
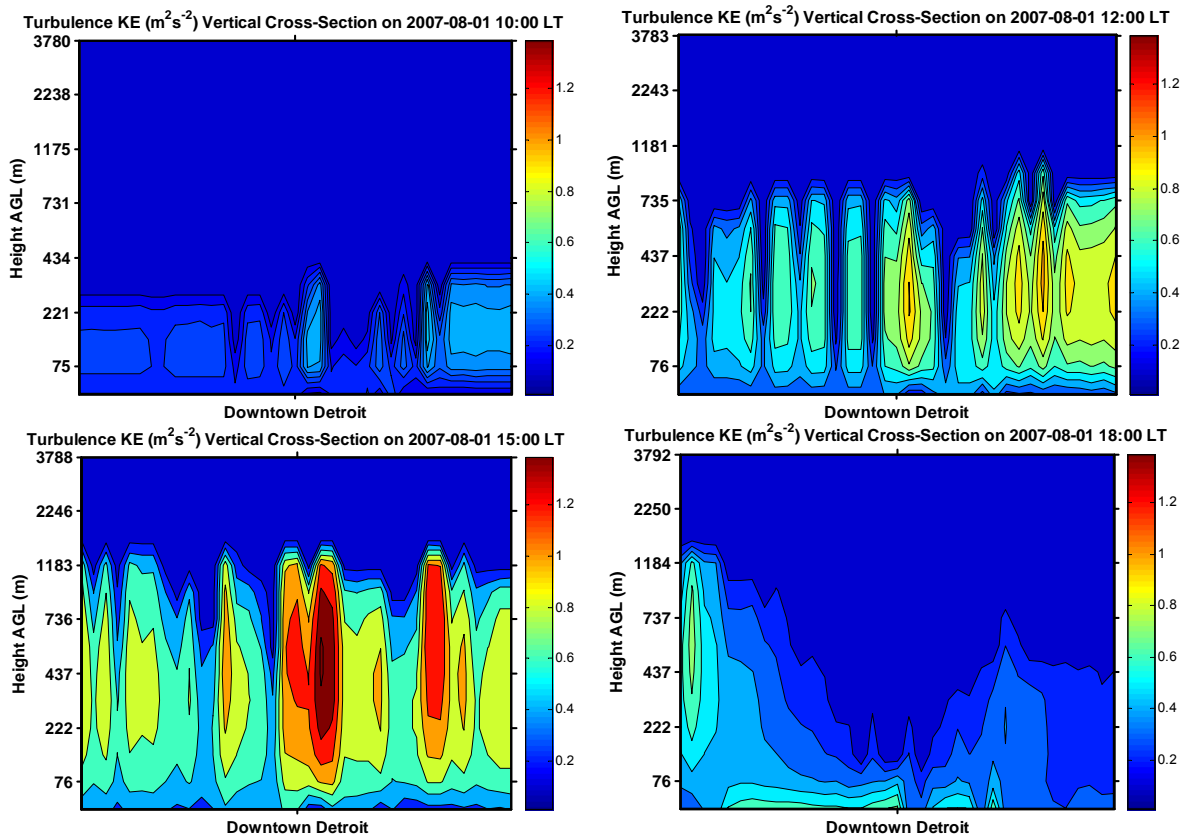
Figures 4-13:

Figure 4: Vertical cross section of turbulence kinetic energy from 16 km NW (left) to 16 SE (right) of downtown Detroit (center) at four points during the growth and decay of the atmospheric boundary layer.
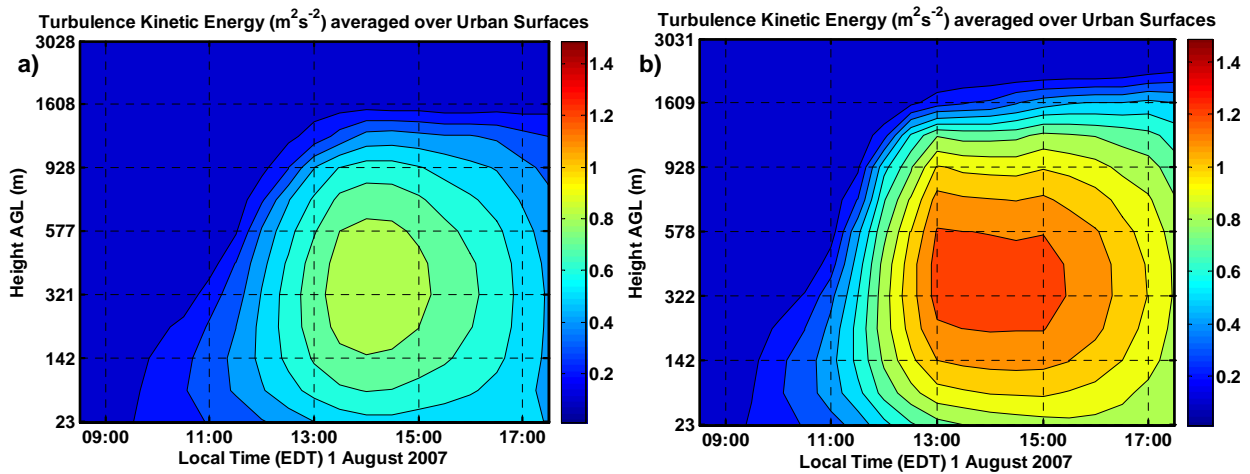

Figure 5: Turbulence kinetic energy averaged over all urban surfaces in domain 3 (see Figure 3) for the "best fit" case (a) and the "no UCM" case (b)
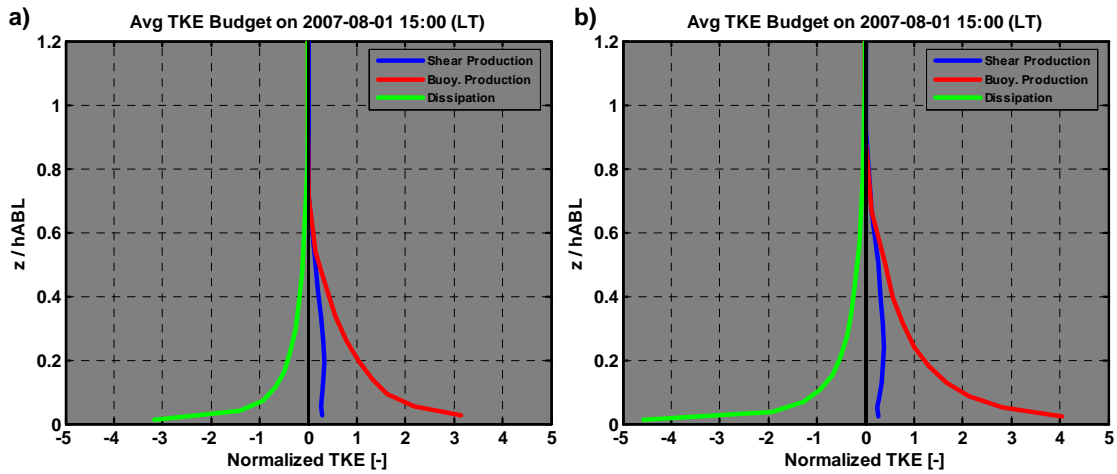
Figure 6: Turbulence kinetic energy budget averaged over all urban surface in domain 3 (see Figure 3) for the "best fit" case (a) and the "no UCM" case (b). Budget components are normalized according to the convective velocity scale (Stull 1988).
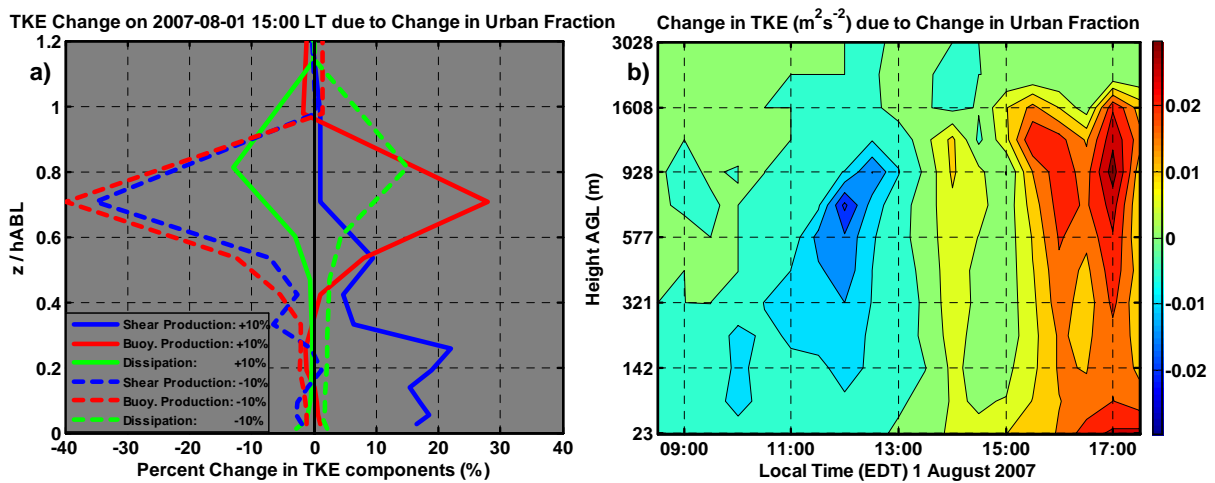
Figure 7: Response of turbulence kinetic energy averaged over all urban surfaces in domain 3 (see Figure 3) to perturbation in the urban fraction parameter; (a) depicts the percent change in the TKE budget components with height at 15:00 LT, (b) illustrates the change in the similarly-averaged TKE profile in time for a +10 percent perturbation in urban fraction.
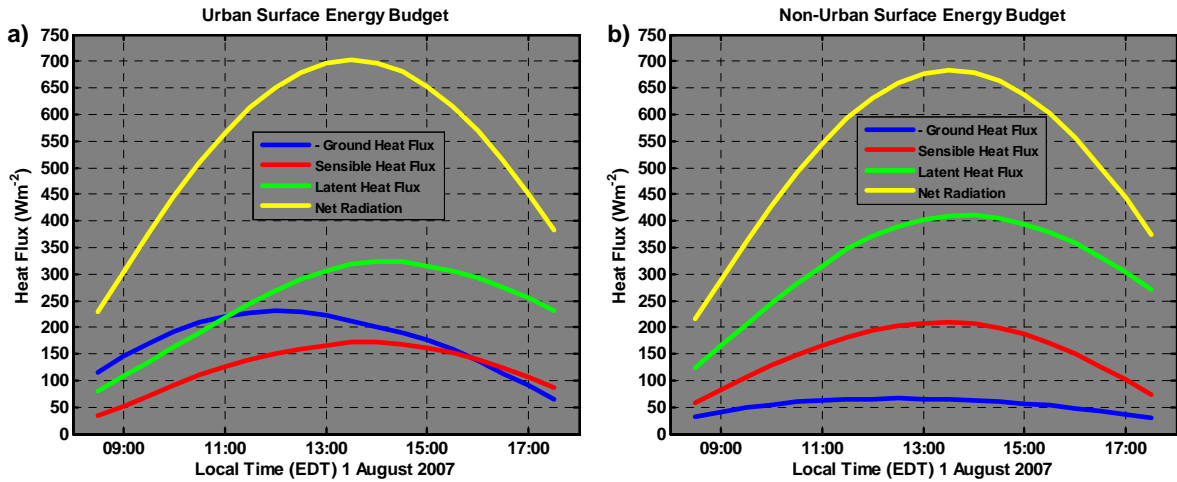
Figure 8: Surface energy budget averaged of all (a) urban surfaces and (b) non-urban surfaces in domain 3.
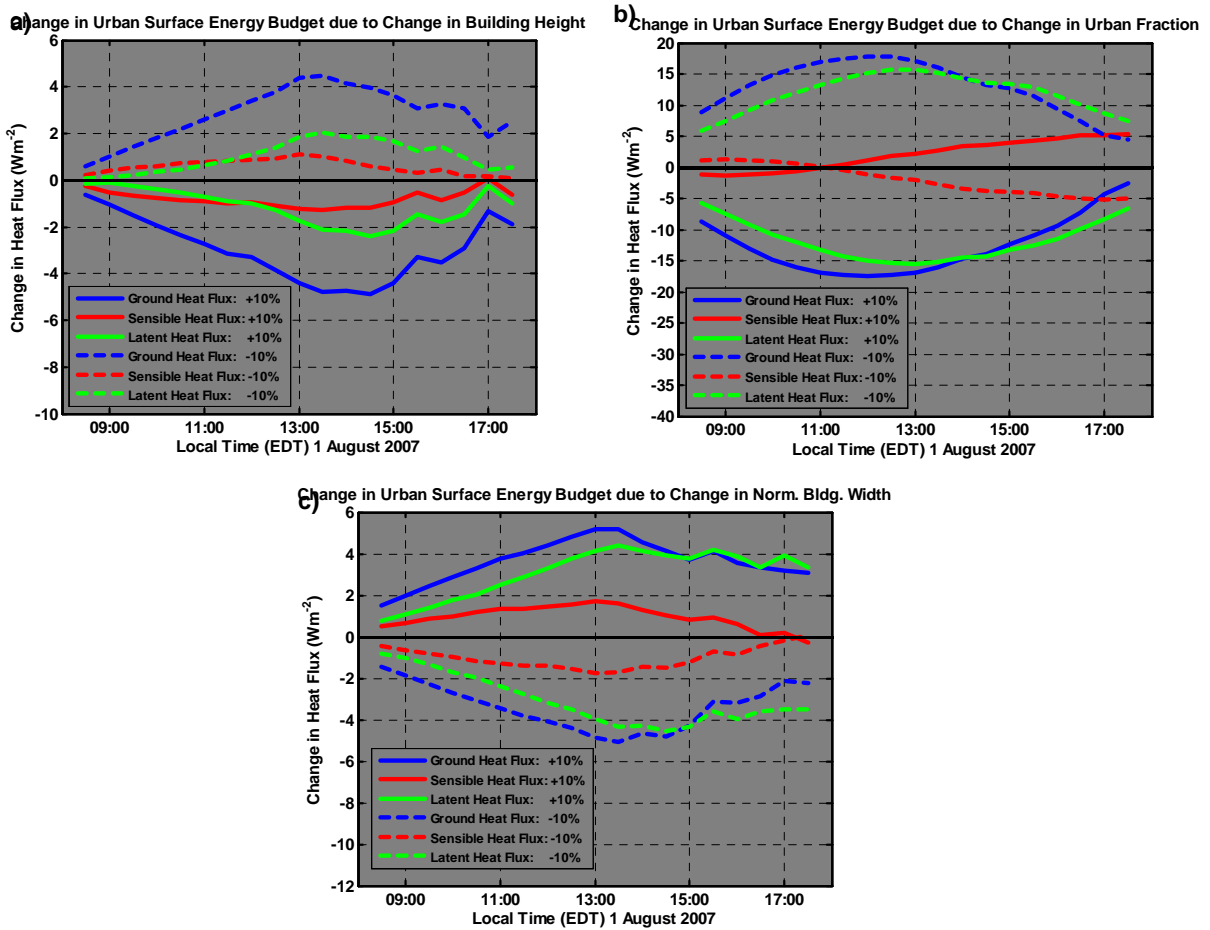

Figure 9: Percent change in surface energy budget averaged over all urban surfaces in domain 3 (see Figure 3) due to 10 percent perturbations in urban morphology parameterization: (a) building height, (b) urban fraction and (c) normalized building width
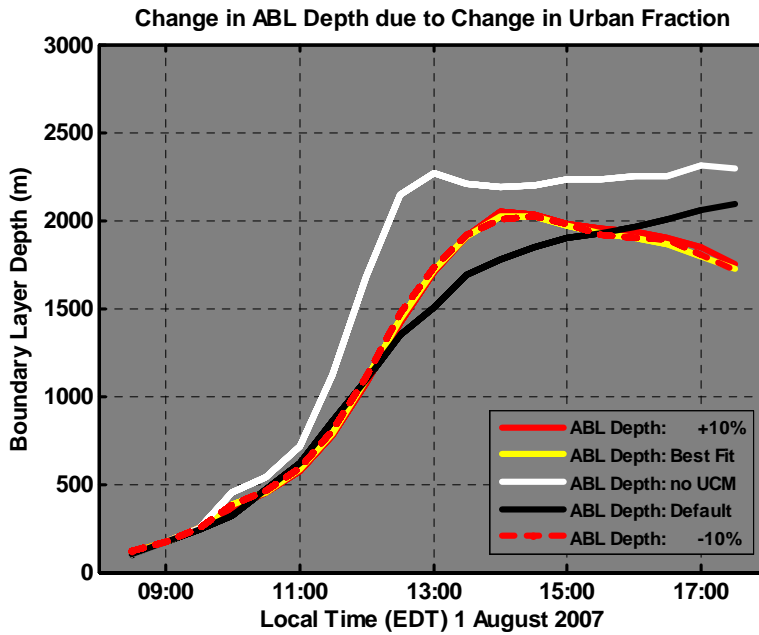
Figure 10: Boundary layer depth averaged over all urban surfaces in domain 3 (see Figure 3) for the "best fit" case (yellow), "no UCM" case (white), 'default' case (black) and the perturbed boundary layer depth due to a 10 percent increase in urban fraction (solid red line) and a 10 percent decrease in urban fraction (dashed red line).
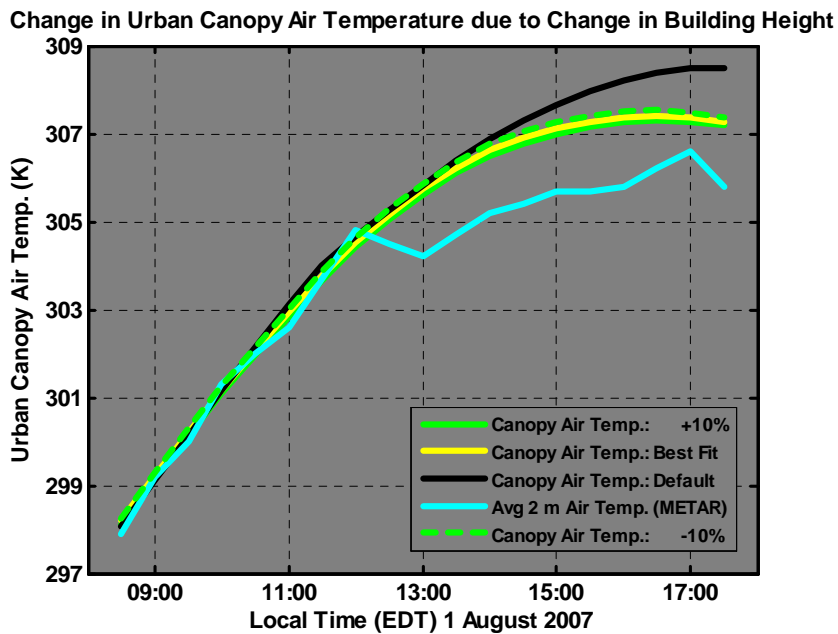

Figure 11: Boundary layer depth averaged over all urban surfaces in domain 3 (see Figure 3) for the "best fit" case (yellow), 'default' case (black), averaged 2 m temperature from local METAR data (blue) and the perturbed boundary layer depth due to a 10 percent increase in building height (solid green line) and a 10 percent decrease in building height (dashed green line).
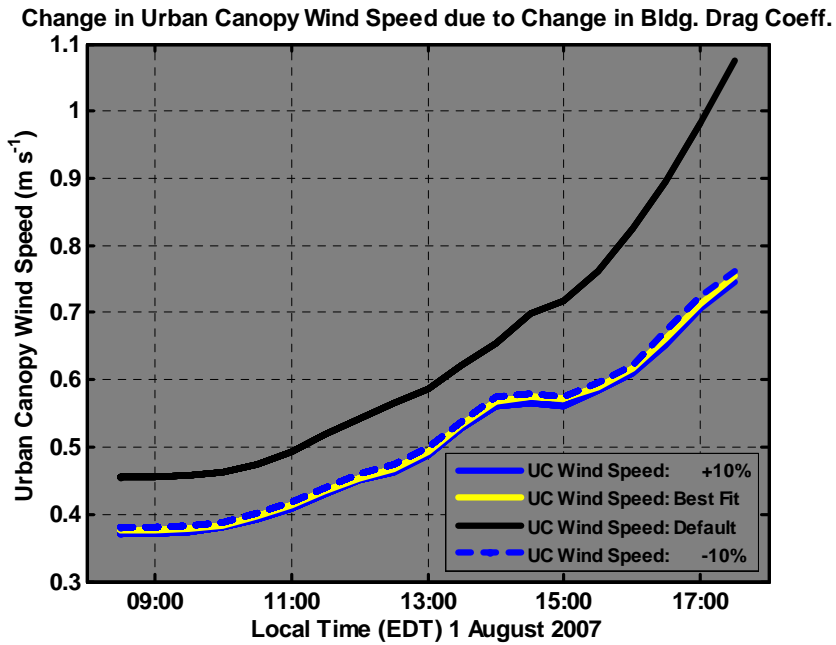
Figure 12: Boundary layer depth averaged over all urban surfaces in domain 3 (see Figure 3) for the "best fit" case (yellow), 'default' case (black) and the perturbed boundary layer depth due to a 10 percent increase in building drag coefficient (solid blue line) and a 10 percent decrease in building drag coefficient (dashed blue line).
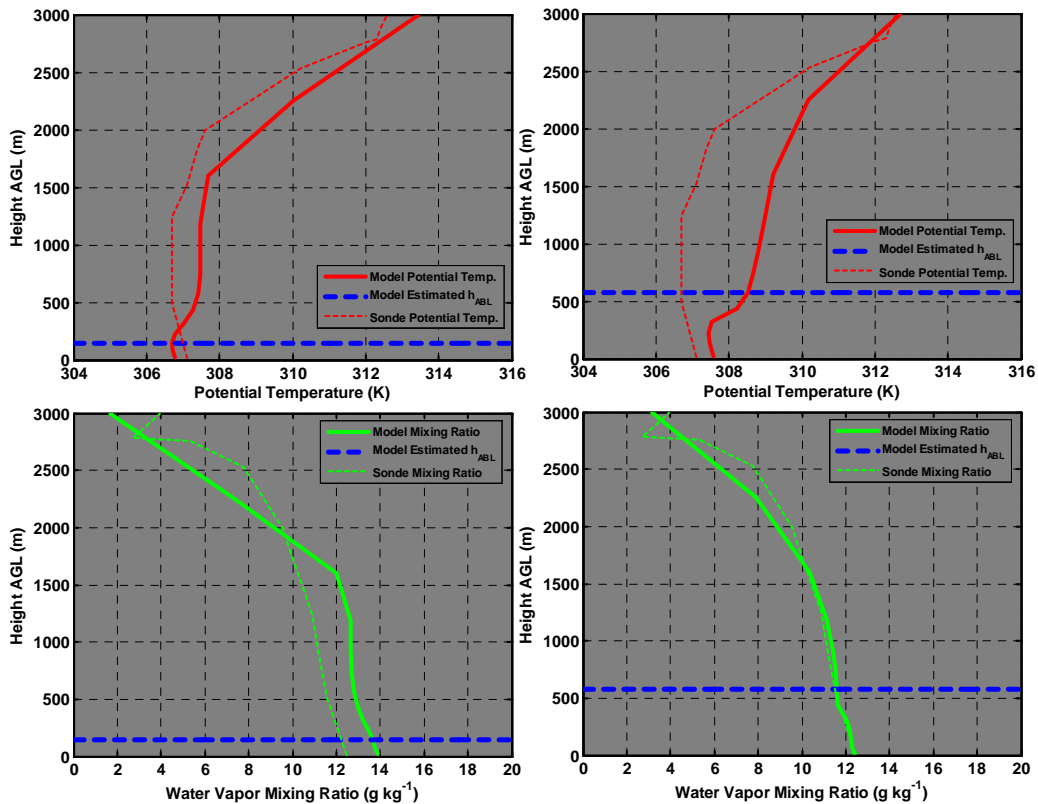

Figure 13: Comparison of model estimates (solid lines) of potential temperature (a,b) and water vapor mixing ratio (c,d) against radiosonde measurements (dashed lines) at KDTX 20:00 LT 01 August 2007, comparing the "best fit" case (a,c) and the "no UCM" case (b,d).